Objective, comparative assessment of the penetration depth of temporal-focusing microscopy for imaging various organs

Christopher J. Rowlands
Oliver T. Bruns
Moungi G. Bawendi
Peter T. C. So

Objective, comparative assessment of the penetration depth of temporal-focusing microscopy for imaging various organs

Christopher J. Rowlands,[a] Oliver T. Bruns,[b] Moungi G. Bawendi,[b] and Peter T. C. So[a,c,*]

[a]Massachusetts Institute of Technology, Department of Biological Engineering, 77 Massachusetts Avenue, Cambridge, Massachusetts 02139, United States

[b]Massachusetts Institute of Technology, Department of Chemistry, 77 Massachusetts Avenue, Cambridge, Massachusetts 02139, United States

[c]Massachusetts Institute of Technology, Department of Mechanical Engineering, 77 Massachusetts Avenue, Cambridge, Massachusetts 02139, United States

Abstract. Temporal focusing is a technique for performing axially resolved widefield multiphoton microscopy with a large field of view. Despite significant advantages over conventional point-scanning multiphoton microscopy in terms of imaging speed, the need to collect the whole image simultaneously means that it is expected to achieve a lower penetration depth in common biological samples compared to point-scanning. We assess the penetration depth using a rigorous objective criterion based on the modulation transfer function, comparing it to point-scanning multiphoton microscopy. Measurements are performed in a variety of mouse organs in order to provide practical guidance as to the achievable penetration depth for both imaging techniques. It is found that two-photon scanning microscopy has approximately twice the penetration depth of temporal-focusing microscopy, and that penetration depth is organ-specific; the heart has the lowest penetration depth, followed by the liver, lungs, and kidneys, then the spleen, and finally white adipose tissue. © The Authors. Published by SPIE under a Creative Commons Attribution 3.0 Unported License. Distribution or reproduction of this work in whole or in part requires full attribution of the original publication, including its DOI. [DOI: 10.1117/1.JBO.20.6.061107]

1 Introduction

Temporal focusing, invented independently by the groups of Oron et al.[1] and Zhu et al.,[2] is a method for performing axially resolved multiphoton excitation of a sample without the need for scanning a focused spot. With sufficient power, large areas can be simultaneously illuminated, allowing high-resolution multiphoton microscopy to be performed with unprecedented frame rates. It works by dispersing an ultrafast pulse using a grating; at any point after the grating, the pulse becomes distorted because each wavelength component has traveled a different distance to that point.[1] Since a transform-limited pulse requires that the wavelength components be substantially in phase with each other in order to maintain a short temporal profile, the pulse becomes broadened in time. As a result, because multiphoton effects are dependent on the instantaneous intensity raised to the relevant power (For example, I^2 in the case of two-photon microscopy), the excitation efficiency of the pulse drops.

The grating is subsequently imaged onto the sample using the microscope tube lens and objective. By the Fermat principle, the imaging system recombines the dispersed color components in phase, reconstructing the ultra-fast pulse. This ensures that excitation occurs primarily in a plane at the grating image location, with a thickness of around 10 μm or less for a microscope objective with a high numerical aperture.[3] The achievable axial resolution has been shown to be very similar to that of two-photon line-scanning microscopy.[4]

It is expected that temporal focusing can excite samples as deep as, if not deeper than conventional two-photon microscopy,[5] but because conventional two-photon laser scanning microscopy can make use of the scattered emission photons in the sample (since all the emitted photons are assumed to come from the focal volume), unlike temporal focusing which can only use the ballistic and weakly scattered photons to form the image, it is expected that in scattering samples such as biological tissue samples, performance will be worse. This paper sets out to characterize the extent of this performance degradation, allowing readers to determine which technique is superior for a given set of imaging conditions.

Currently, attempts to assess the penetration depth of various techniques are highly subjective. Commonly, images are provided at various depths and the reader is left to decide what constitutes an acceptable image or not.[5–7] Another common approach is to measure the emission intensity as a proxy for the penetration depth;[8,9] however, this approach ignores situations where the image is contrast limited, i.e., where the number of collected photons is high, but the image is blurred or it is otherwise impossible to observe the desired features. Some authors have attempted to define a metric based on various image parameters,[10] but the parameters are arbitrary and the threshold is set by defining a similarly arbitrary threshold that corresponds to an "acceptable" image. In one of the only papers to investigate the achievable tissue penetration depth of temporal focusing to date, Papagiakoumou et al.[3] used the cross-correlation of a desired image versus a recorded one, but since the emitted photons were recorded in transmission

*Address all correspondence to: Peter T. C. So, E-mail: ptso@mit.edu

geometry they were not scattered; hence, this experiment cannot be directly described as an investigation of the achievable imaging depth, but only one of the achievable excitation depth.

Given the large number of images that will require comparison, we set out to develop a method that would be based on accepted optical imaging theory, require no user input other than to set some desired target parameters, and to require no 'fudge factors'—any settings must be directly related to the properties of the sample that the user wishes to image.

The modulation transfer function (MTF) is a property of an imaging system that describes the contrast of a given spatial frequency, placed perfectly in focus in the field of view (FOV) and imaged through an optical system. As the spatial frequency increases, the contrast (the intensity ratio between the brightest and darkest points) decreases (see Fig. 1). At the point where the MTF drops to zero, that spatial frequency can no longer be resolved; any features with this spatial frequency cannot be seen. Consequently, this implies that "penetration depth" is user-specific; users who wish to see large features with low spatial frequencies will likely be able to see further into the samples compared to users who wish to see samples with finer features of interest. Therefore, it is helpful to try to estimate the MTF as a function of penetration depth.

The samples used in this paper are Hoechst 34580-stained cell nuclei. These nuclei are small and often have fine features, which provide a high frequency support in the sample. Hoechst 34580 was chosen as an example of a commonly used stain in biological microscopy. Excitation and emission spectra are available from the manufacturer; the emission peaks at approximately 440 nm, decaying to approximately 25% of the peak intensity at 500 nm, but has a very broad tail, extending well past 600 nm. This makes it a good representative fluorophore, as any wavelength-specific scattering or absorption in the sample will affect at least a portion of the emitted light. While an examination of the scattering and absorption cross-sections of different tissues at various wavelengths are beyond the scope of this paper, interested readers are directed to a recent review.[11]

By taking the Fourier transform of an image and taking a "radial average" (i.e., combining all the two-dimensional (2-D)

frequency components with the same frequency, regardless of angle), it is possible to estimate the MTF, assuming that the sample consists of spatial white noise. Clearly, this is only a weak approximation, since the images of the stained nuclei will have a particular spatial frequency content, but the estimate is acceptable for determining the maximum spatial frequency that can be observed in the sample; by determining where the MTF reaches the background level, it is possible to define the maximum spatial frequency and thus, determine the maximum penetration depth for a given desired spatial frequency.

2 Methods

2.1 Sample Preparation

A nine-month-old male Friend Virus B NIH Jackson mouse (Jackson Laboratories) was intraperitoneally injected once with 50 μl of Hoechst 34580 (Life Technologies, 5 mg/ml dissolved in bacteriostatic 0.9% sodium chloride from Hospira), then after a period of 6 h a second dose of 50 μl was intravenously injected. Five minutes after this second injection, the mouse was sacrificed. The organs were harvested and fixated with 2% paraformaldehyde (Electron Microscopy Sciences, 15713-S) dissolved in phosphate buffered saline (Corning, 21-040-CV) for 1 day. For imaging, the organs were mounted with 2% low-melting agarose (Seakem) in a glass bottom dish (Mattek, P35GCOL-1.5-14-C). The dishes were sealed with paraffin film (Bemis Company, Parafilm M) and kept at 4°C until imaging. All mice were housed in an association for assessment and accreditation of laboratory animal care international-accredited facility in the Division of Comparative Medicine at MIT, and were studied according to an approved institutional protocol.

2.2 Temporal Focusing

2.2.1 Instrumentation

The temporal focusing system was constructed around a microscope body (Zeiss, Axiovert S100 TV) with a 20× 1.0 NA water
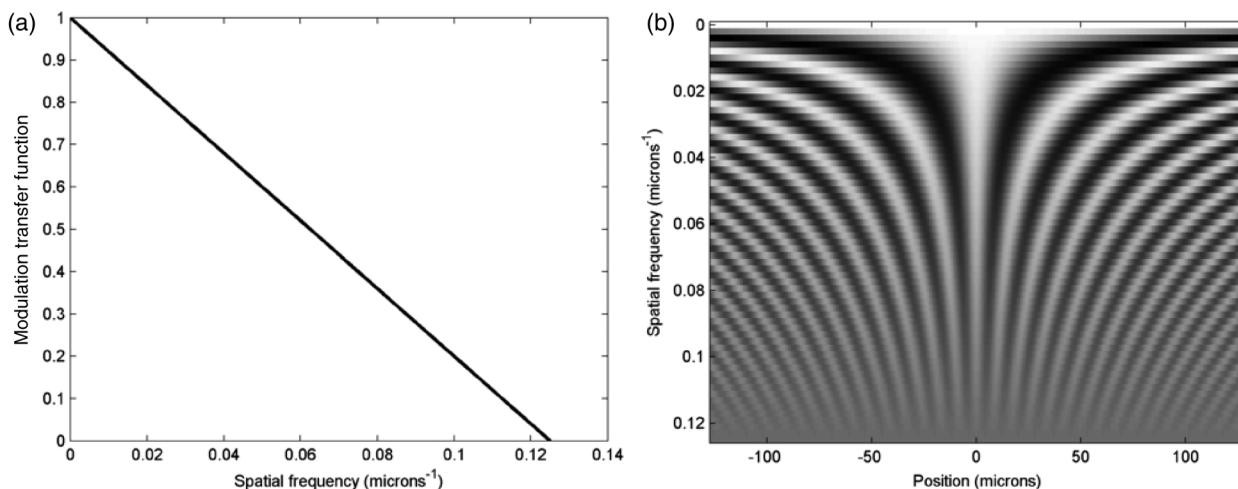
Fig. 1 An illustration of the modulation transfer function (MTF). (a) The MTF as a function of the spatial frequency is plotted. (b) The effect of the MTF on image quality is illustrated. Each row in the image is a cosine function, oscillating between 1 (white) and −1 (black) with the spatial frequency indicated on the *y* axis. The contrast of each cosine function is controlled by the MTF. As the MTF drops, the contrast of the image is reduced. When the MTF drops to zero, the cosine function is no longer visible, as illustrated at the bottom of the image (b).

immersion lens (Zeiss, 421452-9880-000) mounted on a piezo-electric objective stage (Piezosystem Jena MIPOS 500 SG). The fluorescence back port was modified with a tube lens (164.5 mm focal length, Zeiss, 425308-0000-000) such that the image plane lies approximately 30 mm beyond the back of the microscope; excitation light could pass through this back port and be reflected toward the objective by a dichroic mirror. The emission light would pass through the dichroic mirror (Semrock, FF750-SDi02-25x36) and the emission filter (Semrock, FF01-775/SP-25, which served to eliminate any remaining excitation light from the imaging path) toward the camera.

A 50-mm square 1200 lp/mm grating (Richardson Gratings, 53006BK02-540R) was imaged onto this intermediate plane, using a 1.75× beam reducer, consisting of a 2-in. diameter 175-mm focal length, and 30-mm diameter 50-mm focal length lens (Thor Labs, LA1399-B and LA1102-B, respectively) in a 4f configuration. A regenerative (or chirped-pulse) amplifier (Coherent, Legend Elite, seeded by a Mantis oscillator) produced 130 fs pulses at 10 kHz, with a pulse energy of 0.65 mJ per pulse; power was reduced when required using a half wave-plate and polarizing beamsplitter. The wavelength was fixed at 800 nm. The amplifier works by picking a single pulse from the oscillator, stretching it in time using a grating, then amplifying the pulse by several orders of magnitude in a titanium sapphire crystal located in an optical cavity. The resulting amplified pulse is then compressed back to its original pulse duration using a grating compressor.

The pulses were magnified in the vertical axis by 5× using a Galilean cylindrical telescope consisting of a −15-mm focal length lens (Thor Labs, LK1006L1-B) and 75-mm focal length lens (Edmund Optics, 69-762), and projected onto the grating at an angle such that the −1 order diffracted beam propagated along the optical axis of the beam reducer. The magnification ratio was chosen in order to ensure that the image on the grating was approximately circular. Total light throughput from the amplifier to the sample was about 10.7% after the transmission losses through the lenses (especially the objective) and the grating were taken into account.

The bottom port of the microscope was connected to an electron multiplying charge-coupled device (EMCCD) camera (Andor, iXon 885K) to image fluorescence from the sample.

2.2.2 Imaging protocol

The samples were placed on the microscope and visually aligned using the brightfield lamp such that the image plane was approximately at the level of the glass coverslip/sample interface. The lamp was then turned off, the temporal focusing excitation was switched on, and the imaging depth at which the sample just started to be visible was found using the EMCCD and the manual focusing control on the microscope. This step was performed as quickly as possible in order to minimize any potential photobleaching. The focus was then withdrawn a few tens of microns from the sample such that the intensity of the image was close to background levels, and the excitation was turned off. Excitation power was set to 1 W average power at the laser, corresponding to a 107 mW average power at the sample; significantly higher values were found to burn samples. In order to avoid sample damage, tests were performed on a spare piece of liver and the results were assumed to hold for all the other organs. Attempts were made to increase the power once the focal point was within the sample, but no appreciable

increases in incident power could be made without burning the sample.

Z-stacks were taken at 5-μm intervals through the sample using the piezo stage, and were continued until the fluorescence became visually indistinguishable from background. Image resolution was 1004×1002, with each pixel corresponding to 400 nm in the FOV. The integration time was 0.5 seconds per frame. Z-stacks were taken at three different locations for each tissue type. Example data can be seen in Fig. 2.

2.3 Scanning Two-Photon Microscopy

2.3.1 Instrumentation

The scanning two-photon microscope was very similar in design to the temporal focusing system in order to aid comparison between the two. The microscope body (Axiovert S100 TV), objective (Zeiss 421452-9880-000), and piezoelectric objective stage (Piezosystem Jena MIPOS 500 SG) were identical to those in the temporal focusing system, as was the dichroic mirror (Semrock, FF750-SDi02-25x36) and emission filter (Semrock, FF01-775/SP-25). Once again, excitation light was coupled through the back port on the microscope body.
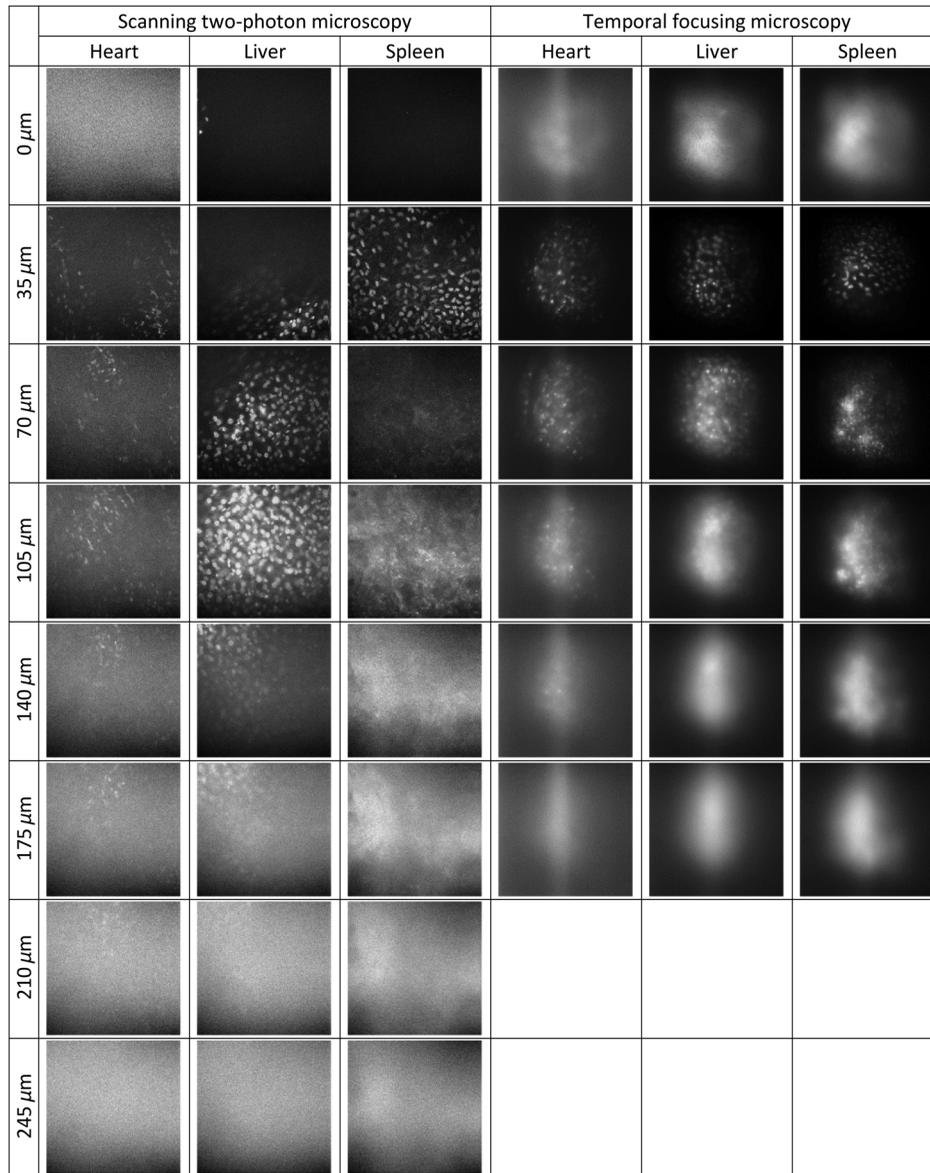
A femtosecond pulsed laser (Spectra Physics, Mai Tai HP) produced pulses at 80 MHz with a pulse duration of <100 fs and a pulse energy of 36 nJ. The wavelength was set to 800 nm using the control software. The beam was passed through an optical isolator (ThorLabs IO-5-NIR-LP) and expanded by a factor of 2 using a pair of lenses (Newport, KPX094AR.16 and KPX106AR.16) in a 4f configuration. The beam then passed through a shutter (Oriel, 76992) before being routed to a pair of scanning mirrors (Cambridge Technology 603X scanning system). The scanning beam was focused onto the image plane using a scan lens (Zeiss, 44132-9901 10× eyepiece, approximately 25-mm focal length); the image was then focused onto the sample using the tube lens (ThorLabs AC254-150-B) and objective. Total light throughput from laser to sample was 33.3%.

After the light had passed the emission filter, it was routed through the microscope body to the camera port where a photon-counting photomultiplier tube (PMT) had been placed (Hamamatsu R7400P-02). The high-voltage power supply for the PMT was custom-designed to be placed as close to the PMT as possible to minimize noise. Signals from the PMT were coupled into a discriminator (Advanced Research Instruments Corporation, F-100T) whereupon they were converted to transistor-transistor logic (TTL) signals.

The instrument was controlled using a data acquisition (DAQ) card (National Instruments PCIe-6321) which was programmed using custom software written using LabVIEW 2013. The DAQ card was responsible for generating the required voltages to control the mirrors as well as counting the TTL pulses corresponding to the arrival of photons at the PMT. Axial resolution, measured by scanning an approximate monolayer of quantum dots through the focus, was determined to be 9.8-μm full width at half maximum.

2.3.2 Imaging protocol

The samples were placed on the microscope and visually aligned using the brightfield lamp such that the image plane was approximately at the level of the glass coverslip/sample interface. The lamp was then turned off, the scanning mirrors

	Scanning two-photon microscopy			Temporal focusing microscopy		
	Heart	Liver	Spleen	Heart	Liver	Spleen
0 μm						
35 μm						
70 μm						
105 μm						
140 μm						
175 μm						
210 μm						
245 μm						

Fig. 2 Selected frames from a series of example Z-stacks. Scanning two-photon field of view (FOV) is 315 × 315 μm and temporal focusing field of view is 401 × 402 μm. Images are scaled to fill the number of displayable intensities.

and laser were switched on, and the imaging depth at which the sample just started to be visible was found using the manual focusing control on the microscope. This step was performed as quickly as possible in order to minimize photobleaching. The focus was then withdrawn a few tens of microns from the sample such that the intensity of the image was close to background levels, and the excitation was turned off.

It was found that for two-photon laser scanning microscopy, the combination of reduced peak power as well as the increased thermal tolerance due to only illuminating one spot at a time, meant that damage thresholds could be avoided if the incident power was increased in stages throughout the imaging process. Therefore, in order to maximize the penetration depth, organ-specific excitation power schemes were used; these are summarized in Table 1.

Z-stacks were taken at 5-μm intervals through the sample and were continued until the fluorescence became visually

indistinguishable from background. The image resolution was 256 × 256 with each pixel corresponding to 1.23 μm in the FOV. The pixel dwell time was 50 μs, which corresponds to an integration time of 3.3 seconds per frame. Z-stacks were taken at three different locations for each tissue type. Example data can be seen in Fig. 2.

In the case of white adipose tissue, images were still observable even at the maximum translation of the stage (400 μm). As such, after a full 400 μm Z-stack was collected, the microscope objective was manually translated 300 μm toward the sample and another full 400 μm Z-stack collected.

2.4 Penetration Depth Assessment Algorithm

Assessment of the penetration depth is based on estimating the MTF as a function of depth. The focal stacks obtained in accordance with the imaging protocols of the two different

Table 1 Power settings used at different penetration depths for each different type of tissues; power levels were selected to maximize signal without causing photodamage.

Sample	Power scheme (power at sample)
Kidney	0 to 100 μm: 33 mW
	100 to 150 μm: 100 mW
	150 to 200 μm: 200 mW
	200 to 250 μm: 333 mW
Liver	0 to 100 μm: 33 mW
	100 to 150 μm: 100 mW
	150 to 200 μm: 200 mW
	200 to 250 μm: 333 mW
Heart	0 to 100 μm: 33 mW
	100 to 150 μm: 100 mW
	150 to 200 μm: 200 mW
	200 to 250 μm: 333 mW
Spleen	0 to 100 μm: 17 mW
	100 to 150 μm: 67 mW
	150 to 200 μm: 200 mW
	200 to 250 μm: 333 W
Lung	0 to 100 μm: 33 mW
	100 to 150 μm: 100 mW
	150 to 200 μm: 200 mW
	200 to 400 μm: 333 mW
White adipose tissue	0 to 300 μm: 33 mW
	300 to 400 μm: 67 mW
White adipose tissue: 300 μm offset	0 to 100 μm: 67 mW
	100 to 200 μm: 200 mW
	200 to 400 μm: 333 mW

instruments were used to generate the data. All processing was performed using MATLAB® 2014a.

The algorithm is described as follows: first, the image is cropped so that it is square. The 2-D fast Fourier transform (FFT) is then taken, and the image is reshaped so that the low-frequency components lie at the center of the image and the high frequency components are at the edge. A "radial average" is then performed, whereby a ring centered on the zero-frequency component is constructed, with a thickness of one FFT pixel. The ring is normalized such that the sum of all pixels in the ring is equal to one, and then multiplied elementwise with the FFT image; the sum over the whole resulting image is then

taken. This summed value is a crude estimate of the MTF at a given spatial frequency. The ring is then enlarged to cover a different spatial frequency, and the process is repeated until the ring is larger than the image. The resulting plot of the estimated MTF versus spatial frequency should have an approximately monotonic decay.

The background level is determined by starting from the highest spatial frequency values and working toward the low frequency values. At each new spatial frequency value, it is compared with the mean and standard deviation of all the previous (higher-frequency) values, which are all assumed to be equal to the baseline plus an individual noise term. If the value of the new point deviates from the mean by more than three times the standard deviation, it is assumed that it is not a noise term, and therefore, is the start of the image information; its value represents the highest observable spatial frequency in that image. The entire algorithm is illustrated in Fig. 3.

The value of three standard deviations were chosen in accordance with the so-called "empirical rule" which states that approximately 99.7% of values drawn from a normal distribution will lie within three standard deviations of the mean; since the noise in this measurement can be approximated as normally-distributed due to the large numbers of photons being captured over the whole image, any values that lie outside this range can reasonably be said to not lie on the baseline. In cases where a more stringent measure of the baseline is necessary, the user may opt for a higher threshold. While the location of the baseline could conceivably be determined by the user, the sheer number of images and the potential for subconscious bias meant that automation was the only reasonable option. Randomly selected images were manually checked, and situations where the image was incorrectly assessed were very rare. As a matter of clarification, the increase in resolution observable at the start of all the Z-stacks is due to the image coming into focus as the microscope objective moves toward the sample. As such, it is broadly consistent between samples and does not reflect an artifact of either temporal focusing or raster-scanning two-photon imaging.

After the "MTF map" has been produced, the user may then decide which spatial frequency they are interested in. In this paper, we use a spatial frequency of 100 lp/mm (corresponding to features 10 μm and larger, which is sufficient to see cell bodies) but readers may select whatever value they like. In the presented data, a magenta line marks the point where the signal drops below the signal-to-background threshold. The outermost points where this magenta line drops below the desired spatial frequency are taken to define the penetration depth. A five-element moving average filter was applied in order to minimize the effect of occasional outliers; the width of this filter was varied from 3 to 9, and the effect on the estimated penetration depths appeared to be minimal.

3 Results and Discussion

Any study such as this one which seeks to assess penetration depth into tissues is inherently limited by the staining of the sample. If, for example, the stain is unable to penetrate into the tissue, or fails to label the cell of interest, then this will be the primary limitation on penetration depth regardless of the instrument performance. In addition, samples may not be stained well near the surface of the organ; since the "start" of the organ is determined by fluorescence, the penetration depth will be underestimated. In this paper, the fluorophore
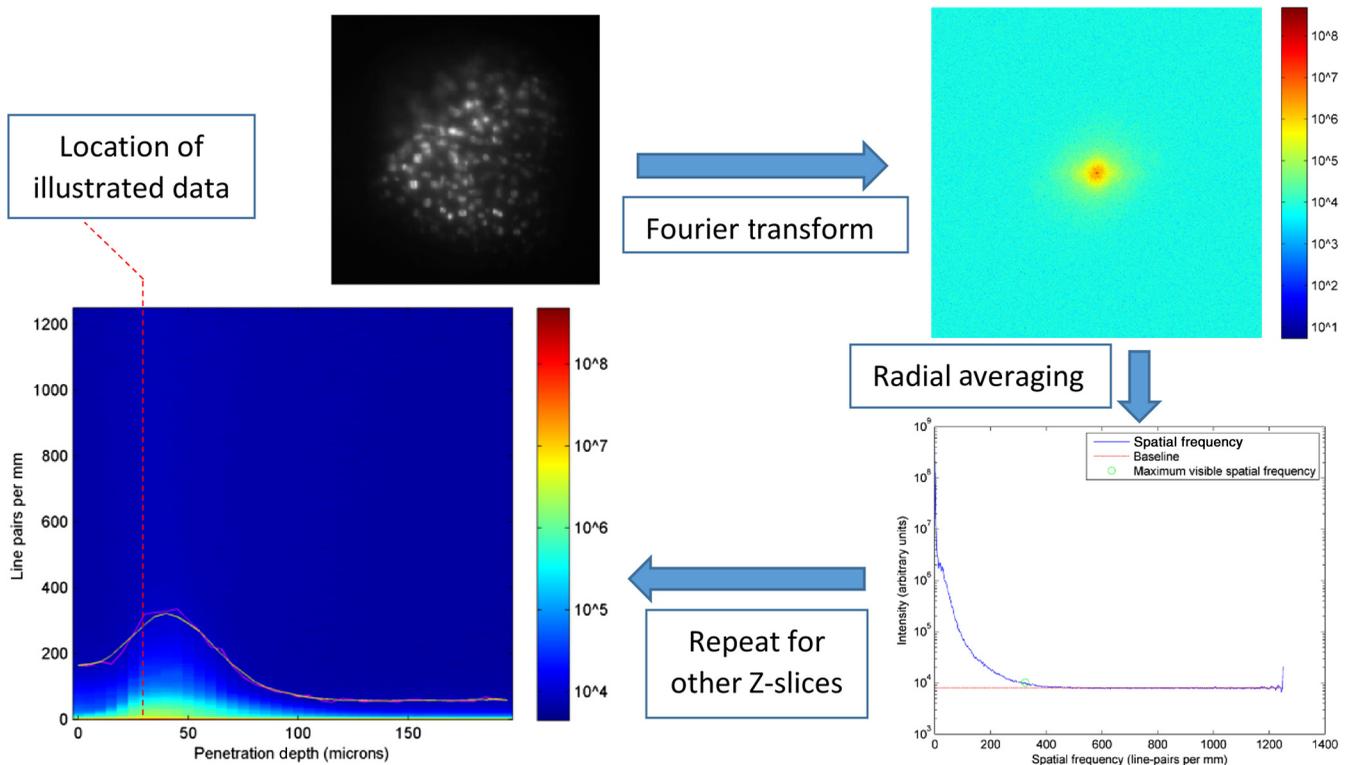
Fig. 3 Illustration of how the penetration depth is estimated using the algorithm developed in this paper. From each image in the Z-stack, the Fourier transform is taken, a radial average is performed, and the baseline is estimated. The highest observable spatial frequency is then found and plotted as a function of penetration depth. Note the logarithmic y axis. The data for all the other Z-positions are then combined, and the maximum observable frequency plotted as a function of depth (magenta line). A five-element moving average filter is applied in order to minimize the effect of any unusual outlier results (yellow line).

was systemically injected in an attempt to minimize these issues, but still they must be considered. As such, we make no claim to be able to assess the maximum penetration depth possible using either temporal focusing or scanning two-photon microscopy; innovative staining protocols and instrumental differences mean that this information would be of limited interest anyway. Rather, we claim to shed light on the relative performance of temporal focusing versus scanning two-photon microscopy, as well as provide some comparison between different tissues.

Another limitation on this study is the differences in staining between organs. The blood–brain barrier prevented us from efficiently imaging the brain, since only a few cells were weakly labeled with Hoechst 34580. Similarly, brown adipose tissue was particularly badly stained. Therefore, these two tissues were rejected from the study as the results were essentially meaningless. The adipose tissues, in general, suffer from the fact that a great deal of their volume consists of lipid droplets; nuclei are effectively squeezed next to the large intracellular lipid droplets. As such, there can be a great deal of variation in apparent penetration depth, depending on whether you are imaging a feature rich in cell nuclei or one with a large proportion of lipid droplets.

With these limitations in mind, it is clear from the data that, depending on the sample, scanning two-photon microscopy can achieve approximately twice the penetration depth of temporal focusing when subject to practical issues such as sample damage (see Figs. 4 and 5, and the data summary in Fig. 6). It was also possible to compare organs in terms of the achievable penetration depth; for the previously mentioned maximum spatial frequency of 100 lp/mm, the heart consistently demonstrated the lowest penetration depth, around 50 μm for temporal focusing and 120 μm for scanning two-photon microscopy. The lungs, liver, and kidneys were all very similar, with penetration depths of approximately 90 μm for temporal focusing and 150 μm for scanning two-photon microscopy. The spleen is slightly easier to penetrate, at around 100 μm for temporal focusing and 180 μm for scanning two-photon microscopy, but the low absorption and scattering due to the large lipid droplets in white adipose tissue meant that penetration depths of nearly 200 μm for temporal focusing and over 500 μm for scanning two-photon microscopy were possible. The especially large error bars were due to the large variation in the measured scanning two-photon penetration depths; values of 190, 635, and 695 μm were recorded, and the 190 μm result strongly skewed the results. This extremely large variation was, in turn, caused primarily by the sparse staining of the sample; the higher resolution of the temporal focusing image made it possible to more readily locate the nuclei, whereas the lower resolution and smaller FOV of the raster-scanning two-photon image meant that the compressed nuclei were harder to distinguish.

The performance of the automated assessment algorithm appeared good, and the metric appeared to accurately reflect a visual assessment of whether a sample can be observed or not. Notably, the "streaks" visible in the plots of Fig. 5, which occurred whenever the laser power was increased, did not
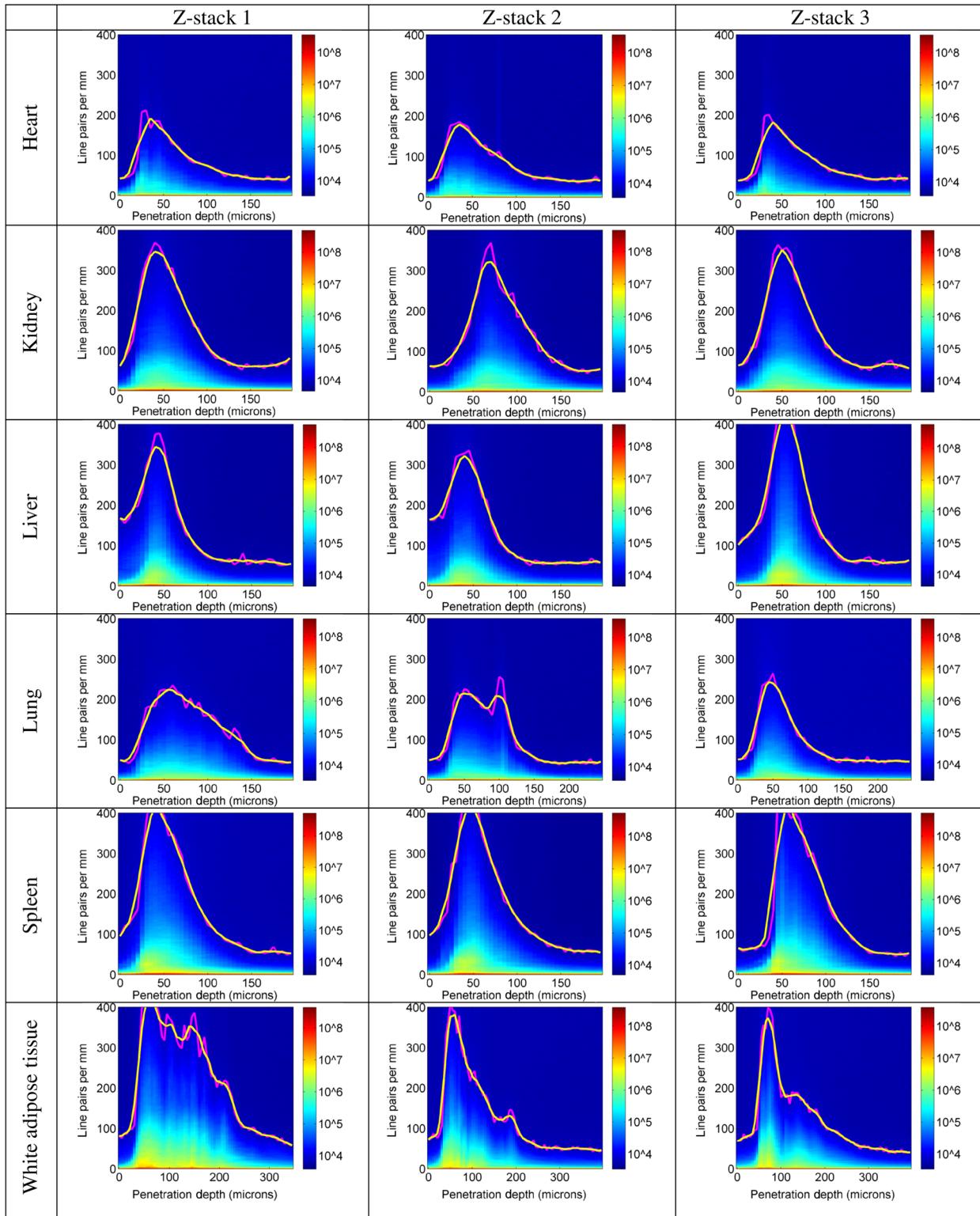
Fig. 4 Penetration depths for temporal focusing. The magenta line indicates the maximum observable spatial frequency as estimated by the algorithm, and the yellow line indicates the result of a five-point moving average filter applied to the raw estimates indicated by the magenta line.

appear to affect the assessment of the maximum observable spatial frequency, which indicates that the algorithm was not affected by image brightness or a reduction in noise; rather it was sensitive primarily to image contrast. During discussions with colleagues, it was proposed that part of the spatial

frequency content was due to nonuniform illumination of the sample. While this is undoubtedly true, this would not invalidate the results in any way, since any projected intensity pattern would become degraded at twice the rate of the sample image, because the light must pass through twice as much tissue.
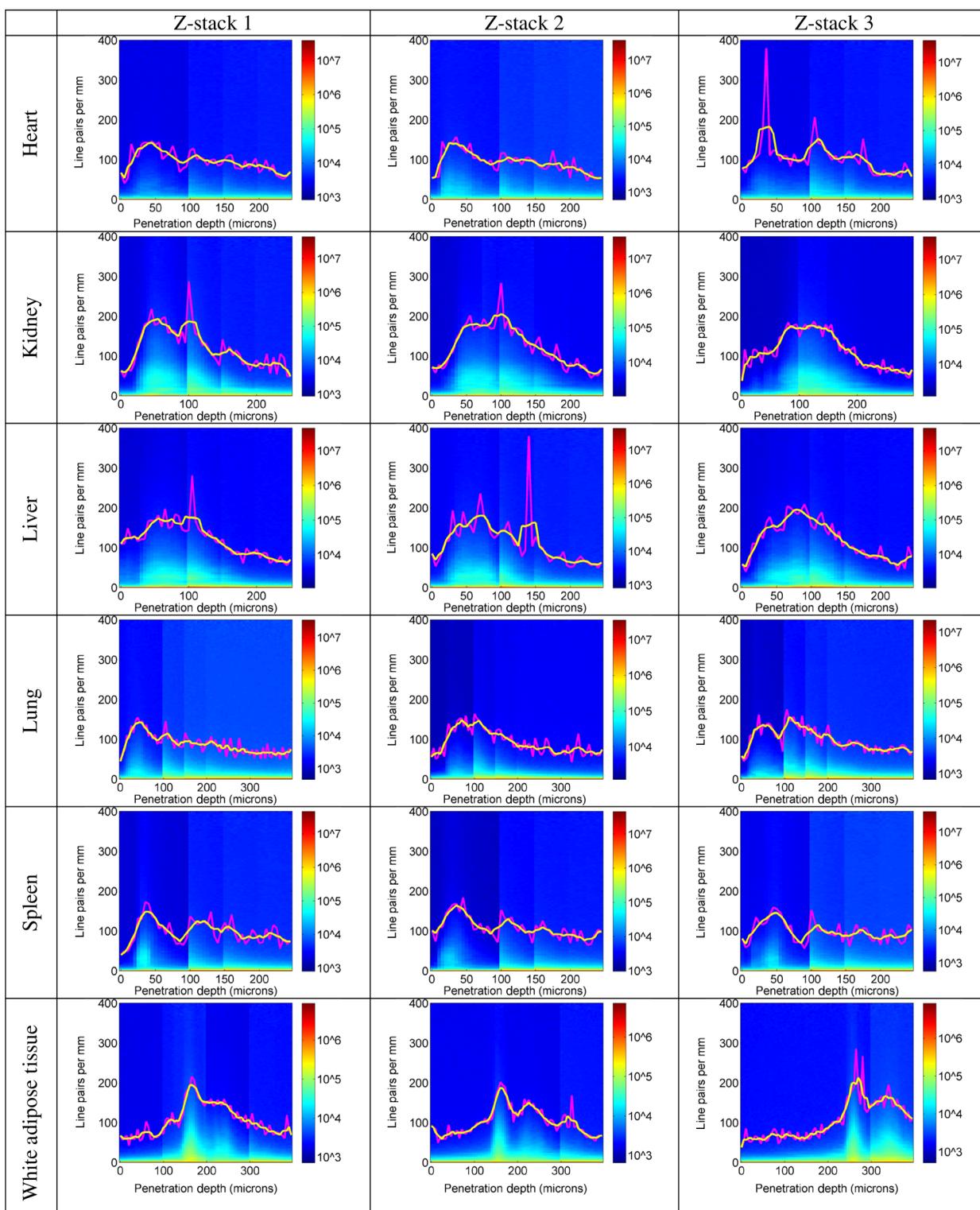
Fig. 5 Penetration depths for scanning two-photon microscopy. The magenta line indicates the maximum observable spatial frequency as estimated by the algorithm, and the yellow line indicates the result of a five-point moving average filter applied to the raw estimates indicated by the magenta line.

In addition, structured illumination would help to locate the start of the sample to a greater degree of accuracy in the case where the start of the sample was comparatively uniform. Nevertheless, an aqueous Fluorescein sample was imaged and analyzed using the automated assessment algorithm in order to provide some context for the presented data. The result was that for the two-photon raster scanning, the maximum observed spatial frequency was 74 lp/mm, and for temporal focusing, the maximum observed spatial frequency was 115 lp/mm. These values are close to the selected 100 lp/mm threshold, hence
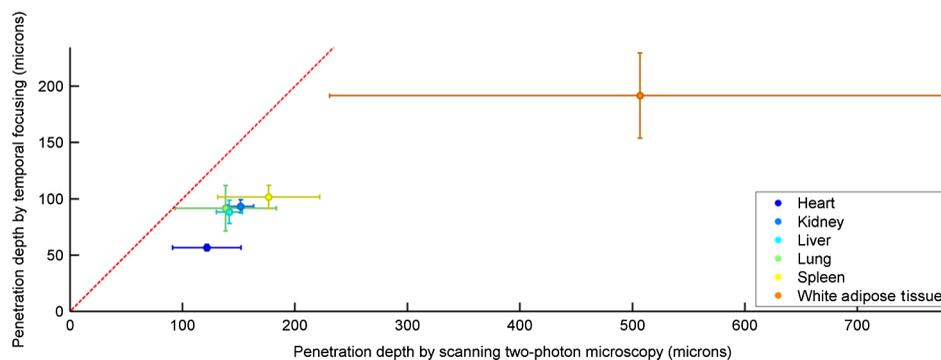
Fig. 6 Comparison between the penetration depth that was achieved using temporal-focusing microscopy and that achieved using scanning two-photon microscopy. Each point corresponds to a different organ. The horizontal coordinate of each point is the mean penetration depth of three Z-stacks obtained using scanning two-photon microscopy, and the error bars indicate the standard deviation of these points. The vertical coordinate and error bars are determined from three Z-stacks obtained in the same manner, but using temporal-focusing microscopy. A dashed line with a gradient of unity and an intercept of zero indicates where points would lie if the penetration depths of temporal-focusing microscopy and two-photon microscopy were equal.

even if the nonuniform illumination were to affect the measured maximum penetration depth, these values would be sufficiently low as to have almost no effect.

Despite the difficulties in using an entirely automated image analysis method, the results appear very encouraging for future use. Measured maximum spatial frequencies on low-resolution images such as the 256×256 scanning two-photon images are noisier than the 1004×1002 images from the EMCCD, which can make determining the penetration depth harder. Nevertheless, with some smoothing, the results appeared largely self-consistent between samples. In addition, the results appeared consistent with visual observation, which provides a sanity check that the automated assessment is accurately reflecting what an observer would see.

4 Conclusion

We have created a method for assessing image quality as a function of depth in tissue samples, and used it to compare temporal-focusing microscopy and scanning two-photon microscopy for a variety of different murine organs. It was found that, in terms of penetration depth, scanning two-photon microscopy consistently outperformed temporal-focusing microscopy by a factor of approximately 2, but at the cost of two orders of magnitude increase in the imaging time. Also, it was possible to gain insight into the penetration depths that were achievable for various organs.

References

1. D. Oron, E. Tal, and Y. Silberberg, "Scanningless depth-resolved microscopy," *Opt. Express* **13**(5), 1468–1476 (2005).
2. G. Zhu et al., "Simultaneous spatial and temporal focusing of femtosecond pulses," *Opt. Express* **13**(6), 2153–2159 (2005).
3. E. Papagiakoumou et al., "Functional patterned multiphoton excitation deep inside scattering tissue," *Nat. Photonics* **7**(4), 274–278 (2013).
4. M. Durst, G. Zhu, and C. Xu, "Simultaneous spatial and temporal focusing in nonlinear microscopy," *Opt. Commun.* **281**(7), 1796–1805 (2008).
5. G. Sela, H. Dana, and S. Shoham, "Ultra-deep penetration of temporally-focused two-photon excitation," *Proc. SPIE* **8588**, 858824 (2013).
6. V. E. Centonze and J. G. White, "Multiphoton excitation provides optical sections from deeper within scattering specimens than confocal imaging," *Biophys. J.* **75**(4), 2015–2024 (1998).
7. S. G. Parra et al., "Multiphoton microscopy of cleared mouse organs," *J. Biomed. Opt.* **15**(3), 036017 (2010).
8. M. Balu et al., "Effect of excitation wavelength on penetration depth in nonlinear optical microscopy of turbid media," *J. Biomed. Opt.* **14**(1), 010508 (2009).
9. C.-Y. Dong et al., "Applications of two-photon fluorescence microscopy in deep-tissue imaging," *Proc. SPIE* **4082**, 105–114 (2000).
10. P. Sarder et al., "Quantitative determination of maximal imaging depth in all-NIR multiphoton microscopy images of thick tissues," *Proc. SPIE* **8948**, 894827 (2014).
11. S. L. Jacques, "Optical properties of biological tissues: a review," *Phys. Med. Biol.* **58**(11), R37–R61 (2013).

Christopher J. Rowlands received his master's in chemistry from Imperial College in 2005 and his PhD in chemistry from Cambridge University in 2010. Afterwards, he undertook a postdoctoral research position in the School of Physics and Astronomy at the University of Nottingham until 2011. He was awarded a Wellcome Trust—MIT Postdoctoral Research Fellowship to join the group of Peter So at MIT in 2011.

Oliver T. Bruns received his diploma in biochemistry/molecular biology in 2005 and his PhD degree in chemistry in 2009 from the University of Hamburg/Germany, where he began to work on bioimaging with nanomaterials. This was followed by two years of

postdoctoral research at Heinrich-Pette-Institute. Bruns joined the group of Moungi Bawendi at MIT in 2011 as a postdoctoral associate.

Moungi G. Bawendi is the Lester Wolfe Professor of Chemistry at MIT. He received his AB in 1982 from Harvard University and his PhD in chemistry in 1988 from The University of Chicago. This was followed by two years of postdoctoral research at Bell Laboratories, where he began his studies on nanomaterials. Bawendi joined the faculty at MIT in 1990, becoming associate professor in 1995 and professor in 1996.

Peter T. C. So holds a bachelor's degree in physics and mathematics from Harvey Mudd College and completed his PhD in physics at Princeton University. He continued his postdoctoral research at the Laboratory for Fluorescence Dynamics at the University of Illinois at Urbana-Champaign. He is currently professor of mechanical and biological engineering at Massachusetts Institute of Technology and is the director of the Laser Biomedical Research Center, a NIH NIBIB research resource.